

Simulating liquid-vapor phase separation under shear with lattice Boltzmann method*

Wang Ce¹ Xu Ai-Guo^{2+ 1} Zhang Guang-Cai² Li Ying-Jun¹

1.China University of Mining and Technology (Beijing), Beijing 100083, China

2. National Key Laboratory of Computational Physics,

Institute of Applied Physics and Computational Mathematics, Beijing 100088, China

We study liquid-vapor phase separation under shear via the Shan-Chen lattice Boltzmann model. Besides the rheological characteristics, we analyze the Kelvin–Helmholtz (K-H) instability resulting from the tangential velocity difference of the fluids on two sides of the interface. We discuss also the growth behavior of droplets. The domains being close to the walls are lamellar-ordered, where the hydrodynamic effects dominate. The patterns in the bulk of the system are nearly isotropic, where the domain growth results mainly from the diffusion mechanism. Both the interfacial tension and the K-H instability make the liquid-bands near the walls tend to rupture. When the shear rate increases, the inequivalence of evaporation in the upstream and coagulation in the downstream of the flow as well as the role of surface tension makes the droplets elongate obliquely. Stronger convection makes easier the transferring of material particles so that droplets become larger.

1 Introduction

Fluidic phenomena in nature are the statistical behaviors of the corresponding microsystems. The thermodynamic properties for a fluid system are determined by kinetic behaviors of the microsystems and the boundary conditions. It is impractical to track fully the evolutions of microsystems using the molecular dynamics (MD) simulation; at the same time, some macro-behaviors are not sensitive to some degrees of freedom. Traditional fluid dynamics does not work well for systems whose nonequilibrium effects are pronounced, for example, the multiphase system. Lattice Boltzmann (LB) method can represent partially the microscopic behavior of a realistic fluid system, and can also be associated with the macroscopic behavior. It is a mesoscopic simulation scheme. The LB method[1] is developed from the lattice vapor automata(LGA)method. Since the LB code has many advantages, for example, it is (i) simple, (ii) easy to deal with complex boundaries, (iii) easy for large-scale parallel computing, etc., it has been attracting more attention with time.

Phase separation of single-component and multicomponent fluids is a fundamental project. It

*Supported by National Natural Science Foundations (under Grants Nos. 10775018、10474137), National Basic Research Program (under Grant No. 2007CB815105) of China, Science Foundations of LCP and CAEP.

¹ Corresponding author.E-mail: Xu_Aiguo@iapcm.ac.cn

is also a project having many applications in a variety of industrial and environmental processes, such as atmospheric quality improving, enhancing oil extraction, underground water purifications, etc[2-10]. LBM is an important tool for simulating the single-phase and multiphase flow. Nowadays, the three well-known LB models for multiphase flows are the Rothman-Kellar model by Gunstensen, et al[11] (1991), Pseudo-potential model by Shan and Chen[12] (1993), and free energy model by Swift et al[13].

The multiphase LB model[14] by Shan and Chen can be used to simulate single-component multiphase flows and component flows. For the latter case, each component can be immiscible and have different masses. The equilibrium state of each component has a nonideal-vapor equation of state. This model introduces interaction forces between particles. Due to collision rules in this model are local, it is highly efficient to compute on massively parallel computers. This model suits for large-scale numerical simulations of various types of fluid flows. Study on multiphase flows and phase separation has a long history[15]. But liquid-vapor phase separation has not got so extensive studies as the phase separations of binary fluid systems. In this study, we apply the Shan-Chen model to study the liquid-vapor phase separation. Besides the rheological behaviors, we analysis the Kelvin–Helmholtz (K-H) instability resulting from the tangential velocity difference of the fluids on the two sides of the interface. We discuss also the growth behavior of droplets.

2 SHAN AND CHEN MODEL

We use the Shan-Chen LB model based on the D2Q9 lattice. The velocity vectors are as follows:

$$\begin{aligned}
 e_i &= (0, 0) \\
 e_i &= \left(\cos \frac{(i-1)\pi}{2}, \sin \frac{(i-1)\pi}{2} \right) c, i = 1, \dots, 4 \\
 e_i &= \sqrt{2} \left(\cos \frac{(2i-1)\pi}{4}, \sin \frac{(2i-1)\pi}{4} \right) c, i = 5, \dots, 8,
 \end{aligned} \tag{1}$$

Where c is the propagation velocity. The particle's distribution function is $f_i(\mathbf{x}, t)$, and its local equilibrium distribution function is $f_i^{eq}(\mathbf{x}, t)$. Under the condition without external force, evolution of the system follows lattice Boltzmann equation:

$$f_i(\mathbf{x} + \mathbf{e}_i, t + 1) - f_i(\mathbf{x}, t) = -\frac{1}{\tau} [f_i(\mathbf{x}, t) - f_i^{eq}(\mathbf{x}, t)] \tag{2}$$

where τ is a single relaxation-time parameter, the local equilibrium distribution functions are:

$$f_0^{eq} = \frac{4}{9} \rho \left[1 - \frac{(\mathbf{u} \cdot \mathbf{u})^2}{2T} \right]$$

$$f_i^{eq} = \frac{1}{9} \rho \left[1 + \frac{(\mathbf{e}_i \cdot \mathbf{u})}{T} + \frac{(\mathbf{e}_i \cdot \mathbf{u})^2}{2T^2} - \frac{(\mathbf{u} \cdot \mathbf{u})}{2T} \right], i = 1, \dots, 4$$

$$f_i^{eq} = \frac{1}{36} \rho \left[1 + \frac{(\mathbf{e}_i \cdot \mathbf{u})}{T} + \frac{(\mathbf{e}_i \cdot \mathbf{u})^2}{2T^2} - \frac{(\mathbf{u} \cdot \mathbf{u})}{2T} \right], i = 5, \dots, 8 \quad (3)$$

where T is the temperature of the system, here $T = c^2 / 3$.

In order to describe the non-ideal vapor or multiphase system, we consider the interaction potential between particles, $V = -\frac{1}{2} G \psi^2$, where $\psi = \rho_0 (1 - \exp(-\rho / \rho_0))$ is an effective density, ρ_0 is the reference density, G is the interaction parameters. Therefore, the interacting force $F = G \psi \nabla \psi$, where the sign of G determines the force is attractive or repulsive. We add external force to the collision term [16]:

$$f_i(\mathbf{x} + \mathbf{c}_i t, t + 1) - f_i(\mathbf{x}, t) = -\frac{1}{\tau} [f_i(\mathbf{x}, t) - f_i^{eq}(\mathbf{x}, t)] + F_i \quad (4)$$

Due to that the velocity vector is fixed in the LB equation, there is a constraint to the external force term in order to ensure the conservations of density and momentum:

$$F_i = w_i \mathbf{e}_i \cdot \mathbf{F} / T \quad (5)$$

where w_i is the weight factor in different directions.

By applying the Chapman-Enskog expansion[17], we can obtain the following Navier-Stokes equations:

$$\frac{\partial \rho}{\partial t} + \nabla \cdot (\rho \mathbf{u}) = 0 \quad (6)$$

$$\frac{\partial (\rho \mathbf{u})}{\partial t} + \nabla \cdot (\rho \mathbf{u} \mathbf{u}) = -\nabla p + \nu \nabla \cdot [\rho ((\nabla \mathbf{u}) + (\nabla \mathbf{u})^T)]$$

where $\nu = (\tau - \frac{1}{2}) c^2 \Delta t / 3$ is the kinematic viscosity, the equation of state reads:

$$p = \rho T - \frac{1}{2} G \psi^2(\rho) \quad (7)$$

Obviously, the pressure is not a monotonic increasing function of density, thermodynamic phase transition may occur in such a system. By setting the first and second orders derivatives of p to be zero,

$$\frac{\partial p}{\partial \rho} = 0$$

$$\frac{\partial^2 p}{\partial \rho^2} = 0 \quad (8)$$

we can obtain the critical point G_c . From the above two equations, we get the following relations:

When $\rho_c = \rho_0 \ln 2$, $T_c = \frac{G\rho_0}{4}$ or $G_c = \frac{4T}{\rho_0}$. It is clear that when the temperature is lower than

T_c or the interaction parameter $G > G_c$, liquid-vapor phase separation occurs.

3 SHEAR BOUNDARY CONDITION

In order to enforce a shear flow on the system, we have used the following scheme. We assume that the shear flow is directed along the horizontal direction. The upper wall velocity is $u = \gamma D / 2$ and moves to the right, where D is the distance between the two walls. The lower wall moves to the left. Let us consider the upper wall (similar considerations apply to the lower wall). After the propagation, the distribution functions $f_1(\mathbf{x}, t)$, $f_2(\mathbf{x}, t)$, $f_6(\mathbf{x}, t)$, $f_5(\mathbf{x}, t)$ and $f_3(\mathbf{x}, t)$ are known on each site, while $f_0(\mathbf{x}, t)$, $f_4(\mathbf{x}, t)$, $f_7(\mathbf{x}, t)$, $f_8(\mathbf{x}, t)$ are not.

From $\sum_i f_i = n$, we get

$$f_4(\mathbf{x}, t) + f_7(\mathbf{x}, t) + f_8(\mathbf{x}, t) = n - (f_0(\mathbf{x}, t) + f_1(\mathbf{x}, t) + f_2(\mathbf{x}, t) + f_3(\mathbf{x}, t) + f_5(\mathbf{x}, t) + f_6(\mathbf{x}, t)) \quad (9)$$

From $\sum_i f_i e_i = n\mathbf{u}$, we get

$$f_7(\mathbf{x}, t) - f_8(\mathbf{x}, t) = n\gamma D / 2c - [f_1(\mathbf{x}, t) + f_5(\mathbf{x}, t) - f_6(\mathbf{x}, t) - f_3(\mathbf{x}, t)] \quad (10)$$

in the x direction and

$$f_4(\mathbf{x}, t) + f_7(\mathbf{x}, t) + f_8(\mathbf{x}, t) = f_2(\mathbf{x}, t) + f_5(\mathbf{x}, t) + f_6(\mathbf{x}, t) \quad (11)$$

in the y direction, where γ is the shear rate. The equation system has three equations with four unknown variables. To close the system of equations the bounceback rule[3] is adopted for the distribution functions normal to the boundary. That is

$$f_2(\mathbf{x}, t) = f_4(\mathbf{x}, t). \quad (12)$$

In order to preserve correctly mass conservation, we add a further constraint. That is,

$$n = \hat{n}$$

$$\begin{aligned} \hat{n}(\mathbf{x}, t - \Delta t) = & f_0(\mathbf{x}, t - \Delta t) + f_5(\mathbf{x}, t - \Delta t) + f_2(\mathbf{x}, t - \Delta t) + f_6(\mathbf{x}, t - \Delta t) \\ & + f_1(\mathbf{x}, t) + f_3(\mathbf{x}, t) + f_2(\mathbf{x}, t) + f_5(\mathbf{x}, t) + f_6(\mathbf{x}, t) \end{aligned} \quad (13)$$

where quantities at time $(t - \Delta t)$ refer to the previous time step and have not been propagated

over the lattice. In order to constrain that on all boundary sites $n = \hat{n}$, we have to introduce an

independent variable in the system of equations. We choose $f_0(t)$ since it does not propagate.

Therefore,

$$\begin{aligned}
f_0(\mathbf{x}, t) &= \hat{n} - [f_1(\mathbf{x}, t) + f_3(\mathbf{x}, t)] - 2[f_2(\mathbf{x}, t) + f_5(\mathbf{x}, t) + f_6(\mathbf{x}, t)] \\
f_4(\mathbf{x}, t) &= f_2(\mathbf{x}, t) \\
f_7(\mathbf{x}, t) &= f_5(\mathbf{x}, t) + \frac{1}{2}[f_1(\mathbf{x}, t) - f_3(\mathbf{x}, t)] - n\gamma D / 2c \\
f_8(\mathbf{x}, t) &= f_6(\mathbf{x}, t) + \frac{1}{2}[f_3(\mathbf{x}, t) - f_1(\mathbf{x}, t)] + n\gamma D / 2c.
\end{aligned} \tag{14}$$

4 SIMULATION RESULTS

With the LB model in Section 2, we choose $T = 1/3$, $\rho_0 = 1/\ln 2$, while $G_c \approx 0.92$. The initial density of system is around 1 with small fluctuations. The lattice size is 256x256, period boundary conditions are used in the horizontal direction and shear boundary conditions are used in the vertical direction. In simulations, we choose $G \approx 0.95 > G_c$. (The corresponding critical temperature is $T_c \approx 0.34$, it is clear that $T = 1/3 < T_c$.)

4.1 Rheological characteristics of liquid-vapor phase

This section is focused on the shear effects on the rheological characteristics of the whole system. What we consider is a temperature quench, which means that the dynamic details occurring in the temperature-decreasing procedure is not taken into account. In Fig.1 and Fig.2 the red color is for liquid phase, and the blue is for vapor. The initial state of the system is set as a constant with tiny fluctuations, corresponding to high temperature uniform single-phase. When the temperature abruptly falls below the critical point and the system enters the parameter regime for two-phase coexistence, the density fluctuations in the system cause the droplets to grow up. Each droplet has a tendency to absorb molecules from the surroundings, in other words, it has the tendency to grow up by diffusion. Since fewer and larger droplets can decrease the interfacial energy, with the evolution, small droplets disappear gradually and the bigger droplets grow with time. The means size of domains of the system increase gradually. As the boundary flow, the droplets nearby can integrate easily with liquid-bands. Since shear effects have not come into the bulk of the system, the domains there are still nearly isotropic. With time going on, the liquid-bands near the walls absorb molecules from the inside and begin to become wider. Both the interfacial tension and the K-H instability make the liquid-bands near the walls tend to rupture. See Fig.1.

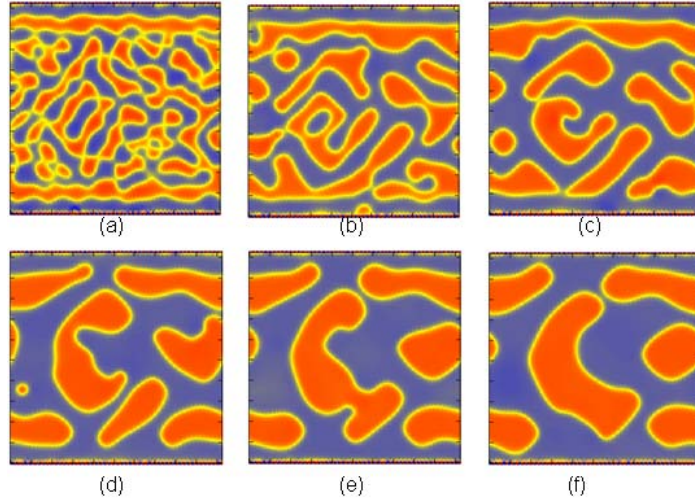


Fig.1 Snapshots for phase separation, where $\gamma = 10^{-5}$. Figs. (a) ,(b) ,(c) ,(d) ,(e) ,(f) correspond to $t=500,1000,1500,2000,2500,3000$, respectively.

With the increase of shear rate, the anisotropic characteristics is more pronounced. Fig.2 shows density configurations for the case of $\gamma = 10^{-4}$. Compared with Fig.1, we can see two differences: when the shear rate increases, the stronger convection makes easier the transferring of material particles so that droplets become larger; the unbalance of evaporation in the upstream and condensation in the downstream of the flow makes the droplets elongated obliquely. (Discuss in details in Sects. 4.4 and 4.5)

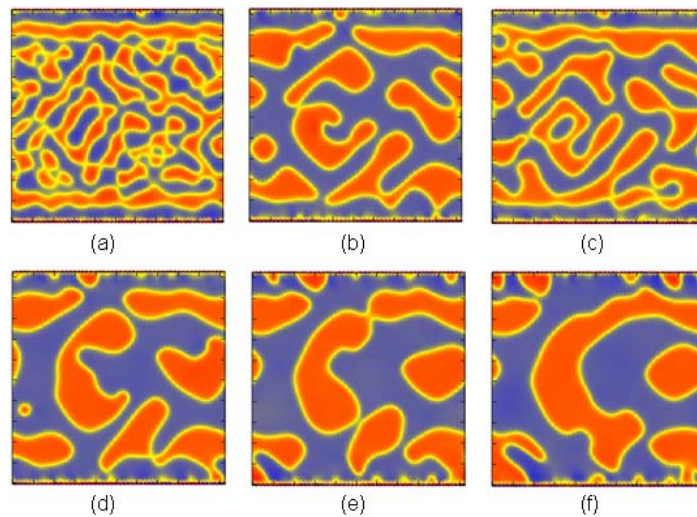


Fig.2 Density configurations for the case of $\gamma = 10^{-4}$. Figs. (a) ,(b) ,(c) ,(d) ,(e) ,(f) correspond to $t=500,1000,1500,2000,2500,3000$, respectively.

The dynamical characteristics of the droplets can be seen via their structure factors. Fig.3 shows the structure factors corresponding to the configurations in Fig.2. In Fig.1 and Fig.2, domains

being close to the walls are lamellar-ordered since the hydrodynamic effects dominate there; the patterns in the bulk of the system are nearly isotropic since the domain growth results mainly from the diffusion mechanism. In Fig.3 ,we can find that, when $t < 500$, the shear makes only some effects close to the walls, correspondingly, the structure factor is nearly circular and isotropic. With time going on, the structure factor becomes elliptic. When $t = 2000$ two peaks appear at $k_x = 0$ along the flow direction. Then the shear effects come into the system. After that the elliptic structure becomes thinner, and the two peaks become more pronounced.

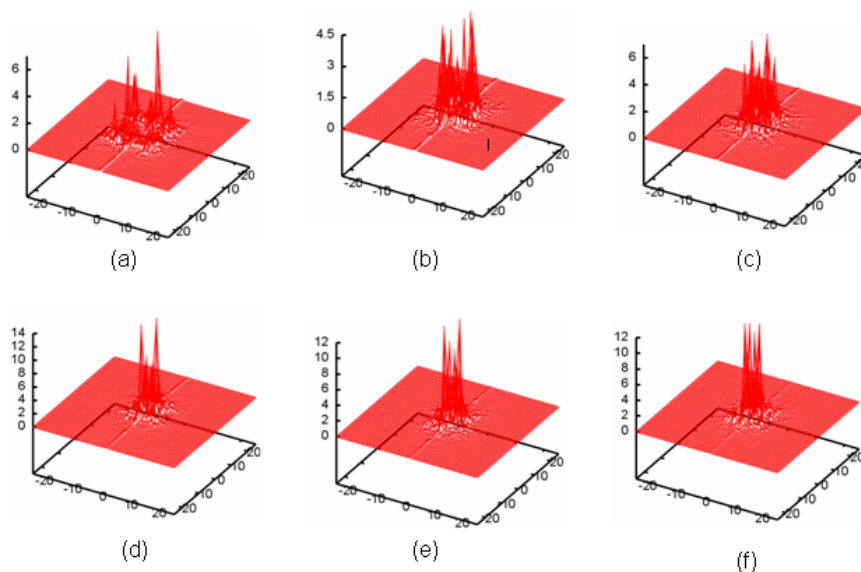


Fig.3 Structure factors for the case of $\gamma = 10^{-4}$. Figs. (a) ,(b) ,(c) ,(d) ,(e) ,(f) correspond to $t=500,1000,1500,2000,2500,3000$, respectively.

4.2 Kelvin–Helmholtz (K-H) instability

In Fig.1 and Fig.2 blue-bands (blue is for vapor) partly prevent the shear effect from entering the system. Then the main transport mechanisms are diffusion and local flow. Near the boundary walls, the flow bands on the two sides of the interfaces have tangential velocity differences, see Fig.4. The tangential velocity difference is the reason for the K-H instability. Together with the interfacial tension, the K-H instability makes thicker the thicker parts and makes thinner the thinner parts of the liquid bands. Finally the liquid bands rupture.

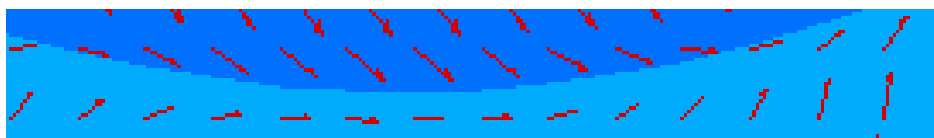
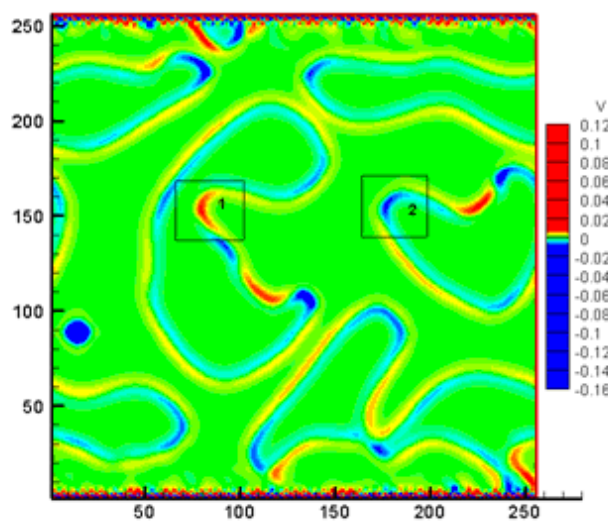


Fig.4 Configuration with velocity field near an interface, where $t=500$.

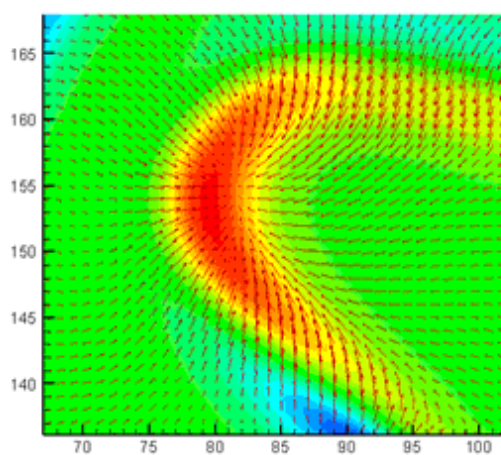
4.3 Mechanism for spherical droplets

In order to study the dynamic characteristics of the droplets, we calculate the spatial distribution of changing rate of density, denoted by v , in Fig.6(a). From Fig.6(a) it is clear that when the droplets' surface curvature is negative, corresponding changing rate of density is positive. The density increasing shows that the vapor in the vicinity of the droplets has a coagulation trend; when the droplets' surface curvature is positive, corresponding changing rate of density is negative. The

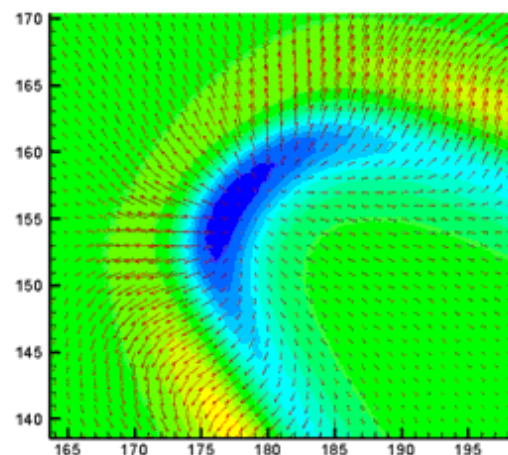
density decrease shows that evaporation occurs at the surface of droplets. Surface tension makes the droplets' surface flatter and flatter. In order to understand better the relationship between congealment (or vaporization) and droplets' surface curvature, we show partial enlarged plots with particle velocity fields in Figs.5(b) and (c). Fig. 5(b) and (c) correspond to regimes in square 1 and square 2 in Figure 5(a). The droplets' surface curvatures are positive and negative, respectively. From Fig.5(b) it is clear that material particles gather to a place where the droplets' surface curvature is negative. From Fig.5(c) we find a reverse process where material particles diverge from a place where the droplets' surface curvature is positive. In Fig.1 we see a round droplet when $t=2000$, its coordinate is from 1 to 25 in x direction, and from 80 to 100 in y direction. Its surface curvature is large, and corresponding changing rate of density is negative, therefore evaporation occurs there. The droplet has completely evaporated when $t=2500$.



(a)



(b)



(c)

Fig.5 Changing rate of density with velocity field, where $t=2000$. Fig. (b) corresponds to the portion in square 1 of Fig. (a). Fig. (c) corresponds to the portion in square 2 of Fig.(a).

4.4 Mechanism of band forming

In Fig.6(a),(b),(c) the color red is for liquid, and blue is for vapor. When the shear rate increases, the banded structure becomes more pronounced with time, see Fig.6(a). After some time the liquid forms an obliquely banded structure in Fig.6 (c). The oblique elongation of band structure results from the unbalance of evaporation in the upstream and coagulation in the downstream of the flow .Figs.6 (d),(e),(f) show the changing rates of density corresponding to Figs. 6(a),(b),(c). The changing rate of density of the liquid is negative in the upstream and is positive in the downstream.

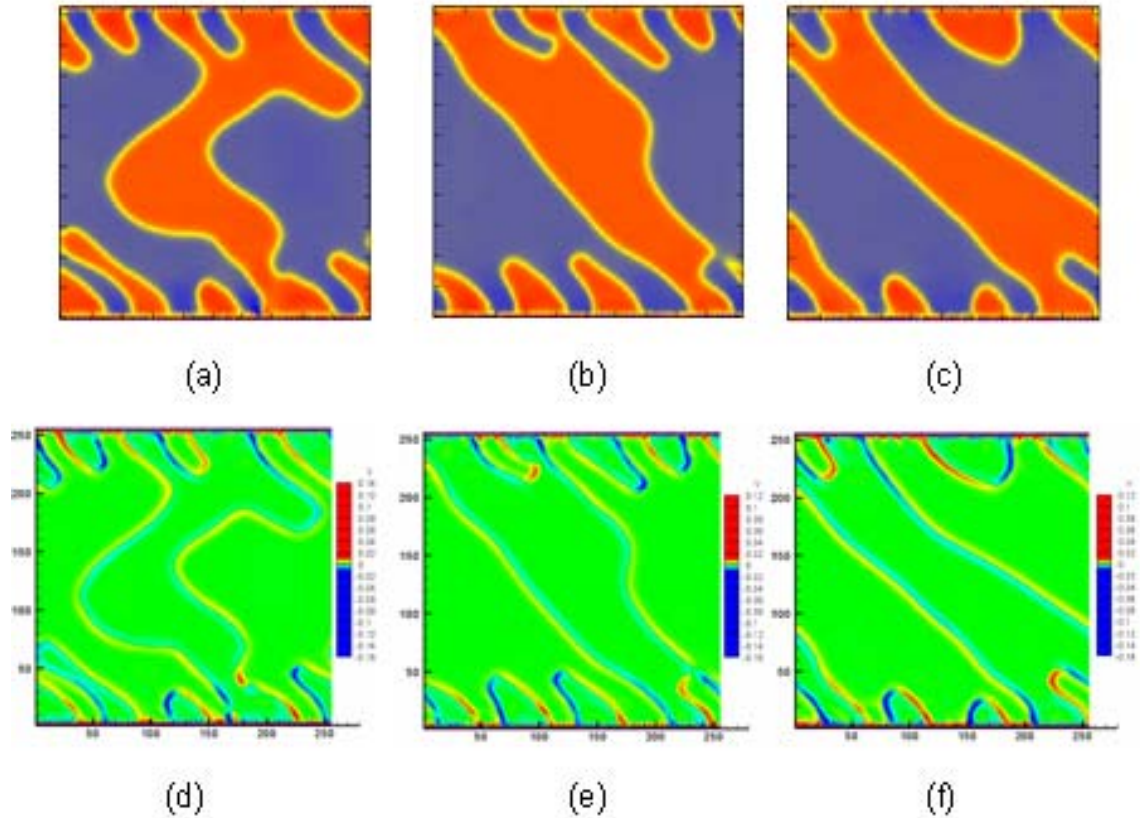


Fig.6 Density and changing rates of density configurations. Figs. (a), (b), (c) show the configurations for the case of $\gamma = 10^{-4}$ at times $t=7000,16000,25000$. Figs. (d),(e),(f) show the changing rates of density corresponding to Figs. (a),(b), (c) .

4.5 Mechanism of droplets on the walls

Compared with Fig.1 and Fig.2, we can see that, when the shear rate increases, it becomes easier for the droplets to grow on the walls. Although droplets on walls can only obtain molecules from one side, stronger convection makes material particles collide and integrate more frequently. Thus, it is easier for the droplets to grow. By tracking the evolution of domains, we can find that, the droplet on the upper wall in Fig.2, located within $150 \leq x \leq 175$ at time $t=500$, can absorb material particles and grow up more easily when convection becomes stronger. The liquid bands near the walls are controlled simultaneously by the surface tension and the K-H instability. Because the K-H instability dominates, the liquid-bands rupture finally.

5 CONCLUSION

We apply the Shan-Chen lattice Boltzmann model to study the liquid-vapor phase separation under shear. We focus on the rheological characteristics, the K-H instability resulting from the tangential velocity difference of the fluids on the two sides of the interface and the growth behavior of droplets. Because the vapor phase transfers the shear effect very weakly, the patterns in the bulk of the system are nearly isotropic, where the domain growth results mainly from the diffusion mechanism. Both the interfacial tension and the K-H instability make the liquid-bands near the walls tend to rupture. When the shear rate increases, the unbalance of evaporation in the upstream and condensation in the downstream of the flow, together with the surface tension, makes the domains elongate obliquely. Stronger convection makes easier transferring of material particles so that droplets become easier to be larger. In the future work, we will investigate the effects of viscosity, oscillatory shear, etc on the rheological behaviors liquid-vapor phase separation. We hope this work will inspire more experimental work.

The authors are grateful to Gan Yanbiao, Wang Lifeng, and Chen Feng for helpful discussions.

- 1 Wolfram S. Cellular automaton fluid 1: Basic theory. *J. Stat Phys*, 1986, 45(2): 471-526
- 2 Yiotis A G, Kainourgiakis M E, Stubos A K. Thermodynamic consistency of liquid-gas lattice Boltzmann methods: Interfacial property issues. *Phys Rev E*, 2008, 78: 036702
- 3 Xu A G, Gonnella G, and Lamura A. Phase-separating binary fluids under oscillatory shear. *Phys Rev E*, 2003, 67: 1103
- 4 Xu A G, Gonnella G, and Lamura A. Phase separation of incompressible binary fluids with lattice Boltzmann methods. *Physica A*, 2004, 331: 10
- 5 Xu A G, Gonnella G, and Lamura A. Numerical study of the ordering properties of lamellar phase. *Physica A*, 2004, 344: 750
- 6 Xu A G, Gonnella G, and Lamura A. Simulation of complex fluids by mixed lattice Boltzmann-finite difference methods. *Physica A*, 2006, 362: 42
- 7 Xu A G. Finite-difference lattice Boltzmann methods for binary fluids. *Phys Rev E*, 2005, 71: 066706
- 8 Xu A G, Gonnella G. Morphologies and flow patterns in quenching of lamellar systems with shear. *Phys Rev E*, 2006, 74: 011505

- 9 Rothman D H, Keller J M.Immiscible Cellular-Automaton Fluids.J Stat Phys,1998,52:1119
- 10 Shan X W,Chen H D.Simulation of nonideal gases and liquid-gas phase transitions by the lattice Boltzmann equation .phys Rev E,1994, 49(4):2941
- 11 Xu A G. Two-dimensional finite-difference lattice Boltzmann method for the complete Navier-Stokes equations of binary fluids.Euro Phys Lett, 2005, 69:214
- 12 Xu A G,Gonnella G, Lamura A,et al. Scaling and hydrodynamic effects in lamellar ordering. Euro Phys Lett, 2005,71:651
- 13 Swift M,Osborn W,Yeomans J. Lattice Boltzman simulation of nonideal fluids.Phys.Rev L ett,1995,75:830
- 14 Shan X W,Chen H D.Lattice Boltzmann model for simulating flows with multiple phases and components. phys Rev E,1993,47(3),1815
- 15 Sofonea V,Lamula A,Gonnella G, et al.Finite-difference lattice Boltzmann model with flux limiters for liquid-vapor systems. Phys Rev E,2004,70:046702
- 16 Guo Z L, Zheng C G,Shi B C.Discrete lattice effects on the forcing term in the lattice Boltzmann method.Phys Rev E 2002,65(47):046308
- 17 Sehgal B R,Nourgaliev R R,Dnh T N,Numerical simulation of droplet deformation and break-up by lattice-Boltzmann method[J].Progress in Nuclear Energy,1999,34:471-478